AJP

ISSN : 0971 - 3093

Vol 24, No 12, December, 2015

ASIAN JOURNAL OF PHYSICS

An International Quarterly Research Journal

ANITA PUBLICATIONS

FF-43, 1st Floor, Mangal Bazar, Laxmi Nagar, Delhi-110 092, India

B O : 2, Pasha Court, Williamsville, New York-14221-1776, USA

ap

Available on www.asianjournalofphysics.in
Invited Article

Asian Journal of Physics Vol. 24, No 12 (2015) 1679-1702

Anamorphic Lohmann's first type system with a non-orthogonal cylindrical doublet. Application to optical encryption

C Ferreira[1], V Micó[1], P García-Martínez[1], I Moreno[2], J García[1], and Z Zalevsky[3]

[1]*Departamento de Óptica y de Optometría y Ciencias de la Visión. Facultat de Física. Universitat de Valencia, C/Doctor Moliner 50, 46100 Burjassot, Spain.*

[2]*Departamento de Ciencia de Materiales, Óptica, y Tecnología Electrónica, Universidad Miguel Hernández, 03202 Elche, Spain.*

[3]*Faculty of Engineering and the Nano Technology Center, Bar-Ilan University, Ramat-Gan 52900, Israel*

Dedicated to Prof Joseph Shamir

A non-orthogonal cylindrical doublet is equivalent to a virtual orthogonal doublet, rotated an angle φ with regard to the original coordinate axes. This angle is a function of the angle α between the cylinder axes of the original doublet and of its focal lengths, as well as of the original orientation of the doublet. Likewise, the focal lengths of the virtual doublet depend on the focal lengths of the original doublet and on the angle α. This property can be used to deal with an anamorphic Lohmann's first -type system (propagation –lens – propagation), where the cylindrical doublet is placed at the same distance from the input and the output planes to obtain a fractional Fourier transform. In this paper, as an application, we propose to use two such systems in cascade to perform double random phase encryption. To introduce different fractional orders in two orthogonal directions and at the same time a rotation of the equivalent system, we only need to rotate one lens of the non-orthogonal doublet in each sub-system. Simulations have been carried out to substantiate the feasibility of the proposed encryption system. Results when angular errors are introduced in each of the sub-systems are shown.

Keywords: Cylindrical doublet, Orthogonal doublet Random phase encryption.

1 Introduction

Sharing information among groups of persons with common interest has been always very important. In many occasions, the information transmitted by different methods must be known only by a restricted number of persons. To do it, researchers have relied on the use of codes. With the passing of time, methods with increasing security are more and more demanded in the last years in several and different areas.

The inherent capability of optical systems for parallel processing is specially fitted for information encoding, in particular for 2D complex data. The information can be encoded using the different parameters that characterize the optical wave. As an additional element of security, Françon and May [1] proposed to use a diffuser in the optical system, which introduces random phase changes. Since then, many optical techniques have been proposed using random masks, either in amplitude or in phase. The results obtained with only one mask didn't reach the level of security expected in principle. Thus, in a pioneering paper, Réfrégier and Javidi proposed the method known as *double random phase encryption* (*DRPE*) [2]. Nowadays, this article is the base for a great number of encoding techniques. In DRPE, using a 4f architecture optical system, the input data are encoded into a stationary white noise by using two statistically independent white noise random phase masks (RPM). The first RPM is introduced in the input plane and the second in the Fourier plane. For the decryption, we must generate the complex conjugates of the two RPMs. In the case that the input data are of amplitude, for the decoding only the complex conjugate of the mask placed in the Fourier

Corresponding author :
e-mail: *Carlos.Ferreira@uv.es.* (C Ferreira)

plane is needed, while with complex data the complex conjugates of both RPMs are necessary. Thus, the method is based on the use of random masks as the encryption keys.

Different modifications of the method were introduced by Javidi *et al* [3-8] to improve the results, just after the publication of that pioneering paper. In [3] the images are represented by phase-only versions, and shows that this nonlinear encryption is more secure than a linear one (amplitude encryption). In [4], digital phase-shifting interferometry is used for efficient recording of amplitude and phase information. The technique can be adapted to encrypt either the Fraunhofer or the Fresnel diffraction pattern of the input. Using a binary spatial light modulator (SLM), in [5] a binary key code is presented to perform shift-invariant encryption and decryption. Encrypted optical storage with wavelength-key is presented in [6] as well as with angular multiplexing in [7]. In [8] fully phase encryption is used to obtain a secure holographic memory. They proposed also to employ digital holography to encrypt three-dimensional information [9], as well as the use of a joint transform correlator (JTC) architecture [10]. Concerning the use of digital holography, recently it has been reported a novel technique for personal authentication [11] in which fingerprint images are captured using an optical encryption method similar to that in Ref [9]. Concerning the JTC architecture, the interest is based on its robustness and on the fact that it does not require an accurate optical alignment. In the context of optical encryption, to record fully complex information, it is necessary to employ holographic methods, so it is necessary to introduce a reference wave. A classical arrangement could be a Mach-Zehnder interferometer with the JTC in one arm and the reference in the other. Nevertheless, recently it has been published an article where the external reference wave is avoided [12].

In order to increase the security, Unnikrishnan *et al* [13,14] proposed to perform the encryption with fractional Fourier systems adding more keys in the form of fractional orders. Since then, the fractional Fourier transform (FRFT) [15-25] is usually applied in image encryption. For the decryption is now necessary to know the correct fractional order besides the conjugates of the RPMs. The optical implementation has been performed with either Lohmann's first-type or Lohmann's second-type systems [15,20].

After the introduction of fractional Fourier systems, methods based on iterative fractional Fourier transform have been proposed [26,27], as well as encoding in the Fresnel domain [28]. Many papers have been published since then in the field following these ideas. For instance, encryption obtained by combining digital holography and the joint transform correlator architecture [29] or double image encryption combining fractional Fourier domain and pixel scrambling technique [30] or linear blend operation [31]. In a recent review paper [32], the authors describe a good number of the optical image encryption techniques proposed in the literature. They also provide a great number of related references.

As next step, the use of anamorphic fractional Fourier transformers [33-36] in the DRPE provides the encoding of a 2D image with two different fractional orders in two orthogonal directions [37], using cylindrical lenses in Lohmann's bulk systems. As a way to add some more security, Kumar *et al* [38] proposed to use as anamorphic system two Lohmann's second type in cascade, where the spherical lenses have been replaced by pairs of orthogonally aligned cylindrical lenses, adding an in-plane rotation of the pairs of cylindrical lenses between the input plane and the Fourier plane, an another in-plane rotation, which can be different from the previous one, between the Fourier plane and the final plane. These rotations constitute extra encryption keys. However, the experimental setup looks not to be very robust and versatile due to the eight cylindrical lenses and the additional constraint of rotating the two parts of the system: losing the alignment could result in uncorrected decryption.

In this paper, we propose the use of an anamorphic Lohmann's first-type system (propagation-lens-propagation) with a non-orthogonal cylindrical doublet placed at the same distance from the input and the output planes in each of the two FRFT subsystems. Each non-orthogonal doublet is equivalent to a virtual

orthogonal doublet, rotated an angle φ with regard to the original coordinate axes [39,40]. This angle is a function of the angle α between the cylinder axes of the original doublet and of its focal lengths, as well as of the original orientation of the doublet. Likewise, the focal lengths of the virtual equivalent doublet depend on those focal lengths and on the angle α. To introduce different fractional orders and at the same time a rotation of the equivalent system, we only need to rotate one lens of the non-orthogonal doublet in each sub-system.

In Section 2, we present the mathematical analysis, in matrix formalism, of both the anamorphic Lohmann's first type system with a non-orthogonal cylindrical doublet to obtain the FRFT of an input image and the system that we propose for optical encryption based on DRPE method. Section 3 gives computer simulation results to verify the feasibility of the system and its flexibility. Finally, Section 4 contains the main conclusions of the work.

2 Mathematical Analysis

2.1 Anamorphic Lohmann's type I system with a non-orthogonal cylindrical doublet.

Shorter after the initial works on FRFT with grin lenses, Lohmann [15] proposed two bulk systems producing FRFT, nowadays known as Lohmann's type I and type II systems. The first type system consists of a free propagation of distance *d,* a converging spherical lens of focal length f', and a second free propagation of distance *d,* as shown in Fig 1(a).

In matrix notation [25], this system can be described by

$$M_{LohI}=\begin{pmatrix}1 & d\\ 0 & 1\end{pmatrix}\begin{pmatrix}1 & 0\\ -\frac{1}{f'} & 1\end{pmatrix}\begin{pmatrix}1 & d\\ 0 & 1\end{pmatrix}=\begin{pmatrix}1-\frac{d}{f'} & d\left(2-\frac{d}{f'}\right)\\ -\frac{1}{f'} & 1-\frac{d}{f'}\end{pmatrix} \tag{1}$$

We compare this matrix with the general matrix of an optical system performing a FRFT, of order *p*

$$M_{FRFT}(p)=\begin{pmatrix}\cos\Phi & f_1\sin\Phi\\ -\frac{\sin\Phi}{f_1} & \cos\Phi\end{pmatrix} \tag{2}$$

where the fractional order *p* is given by the angle $(\varphi - p\pi/2)$.The parameter f_1 acts as a scaling factor. Sometimes, this parameter is referred to as the *standard or generalized focal length,* although we note that the focal length of the FRFT system is given by $f' = f_1/\sin\varphi$.

From Eqs (1) and (2), we see that

$$\cos\Phi = 1-\frac{d}{f'} \tag{3a}$$

$$f_1\sin\Phi = d\left(2-\frac{d}{f'}\right) \tag{3b}$$

$$f' = \frac{f_1}{\sin\Phi} \tag{3c}$$

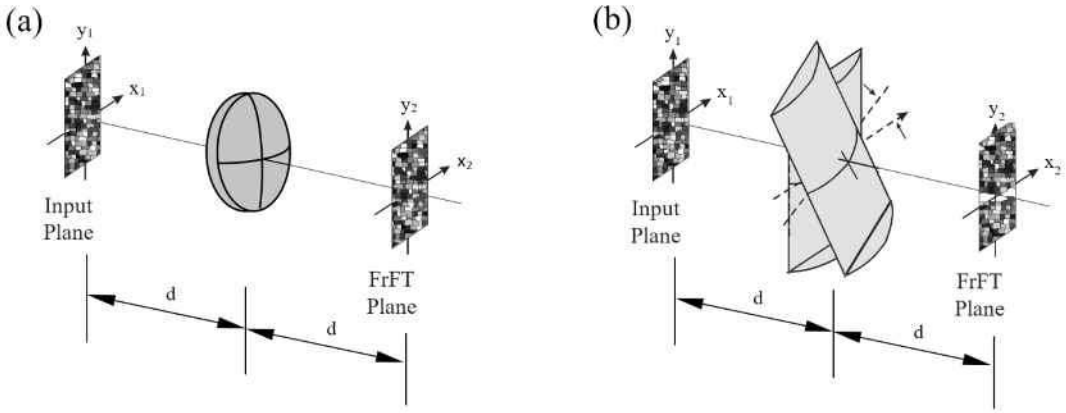

Fig 1. Schemes of Lohmann's first type fractional Fourier transform systems: (a) spherical lens configuration and (b) anamorphic with a non-orthogonal cylindrical doublet architecture.

The application of the Collins formula [25] to this ray matrix provides the output FRFT field, $g_2(x_2, y_2)$, as a function of the input field, $g_1(x_1, y_1)$:

$$g_2(x_2,y_2)=FRFT^p\left[g_1(x_1,y_1)\right]=\frac{1}{j\lambda\sin\Phi}\exp\left(j\pi\frac{x_2^2+y_2^2}{T}\right)\cdot$$
$$\iint g_1(x_1,y_1)\exp\left(j\pi\frac{x_1^2+y_1^2}{T}\right)\exp\left[-j2\pi\left(\frac{x_1x_2+y_1y_2}{S}\right)\right]dx_1dy_1 \tag{4}$$

where: $S=\lambda f_1\sin\Phi$ (5a) and $T=\lambda f_1\tan\Phi$ (5b)

The generalization to an anamorphic system, where the spherical lens has been replaced by a pair of orthogonal cylindrical lenses, with focal lengths f'_x and f'_y, aligned with the coordinate axes x and y is straightforward. The ray matrix becomes now a 4 × 4 matrix.

$$\begin{bmatrix} 1-\frac{d}{f'_x} & d\left(2-\frac{d}{f'_x}\right) & 0 & 0 \\ -\frac{1}{f'_x} & 1-\frac{d}{f'_x} & 0 & 0 \\ 0 & 0 & 1-\frac{d}{f'_y} & d\left(2-\frac{d}{f'_y}\right) \\ 0 & 0 & -\frac{1}{f'_y} & 1-\frac{d}{f'_y} \end{bmatrix} \tag{6}$$

And the FRFT is given by

$$g_{2An}(x_2,y_2)=FRFT_x^{p_x}FRFT_y^{p_y}\left[g_1(x_1,y_1)\right]\propto\iint g_1(x_1,y_1)\exp\left[j\pi\left(\frac{x_2^2+x_1^2}{T_x}\right)\right]\cdot$$
$$\exp\left[j\pi\left(\frac{y_2^2+y_1^2}{T_y}\right)\right]\exp\left[-j2\pi\left(\frac{x_1x_2}{S_x}+\frac{y_1y_2}{S_y}\right)\right]dx_1dx_2 \tag{7}$$

$$S_x = \lambda f_{1x} \sin \Phi_x \tag{8a}$$

$$T_x = \lambda f_{1x} \tan \Phi_x \tag{8b}$$

$$\Phi_x = p_x \frac{\pi}{2} \tag{8c}$$

$$S_y = \lambda f_{1y} \sin \Phi_y \tag{9a}$$

$$T_y = \lambda f_{1y} \tan \Phi_y \tag{9b}$$

$$\Phi_y = p_y \frac{\pi}{2} \tag{9c}$$

In this article, we propose to replace the spherical lens of the orthogonal Lohmann's type I system by a non-orthogonal cylindrical doublet of focal lengths f_1' and f_2', the cylinder axes making the anglesα_1 and α_2 with the x-coordinate axis, respectively, as shown in Fig 1(b). If we call $\alpha = \alpha_2 - \alpha_1$, such a non-orthogonal doublet, as was established by Long for the dioptric power matrix [39] and by Macukow and Arsenault [40] for the ray matrix, is equivalent to an orthogonal doublet of focal lengths f_A' and f_B', given by

$$\frac{1}{f_A'} = \frac{1}{2f_1'} + \frac{1}{2f_2'} + \frac{1}{2}\sqrt{\frac{1}{f_1'^2} + \frac{1}{f_2'^2} + \frac{2\cos(2\alpha)}{f_1' f_2'}} \tag{10a}$$

$$\frac{1}{f_B'} = \frac{1}{2f_1'} + \frac{1}{2f_2'} - \frac{1}{2}\sqrt{\frac{1}{f_1'^2} + \frac{1}{f_2'^2} + \frac{2\cos(2\alpha)}{f_1' f_2'}} \tag{10b}$$

and rotated an angle φ with regard to the *x*-axis, given by

$$\tan\varphi = \frac{Cf_1'f_2' - f_2'\cos(2\alpha_1) - f_1'\cos(2\alpha_2)}{f_2'\sin(2\alpha_1) + f_1'\sin(2\alpha_2)} \tag{11a}$$

$$C = \pm\left[\frac{1}{f_1'^2} + \frac{1}{f_2'^2} + \frac{2\cos(2\alpha)}{f_1' f_2'}\right]^{1/2} \tag{11b}$$

When the cylinder axis of one of the lenses of the doublet is aligned with a coordinate axis, Eq (11a) simplifies to

$$\tan(2\varphi) = \frac{f_1'\sin(2\alpha)}{f_2' + f_1'\cos(2\alpha)} \tag{11c}$$

The ray matrix of this virtual doublet referred to the *x*- and *y*-axes is no longer a diagonal block matrix as that given by Eq (6), so in the anti-diagonal blocks some elements are different from zero and the system cannot be treated as two independent systems in the *x*- and *y*-directions. But if we refer to a new coordinate system rotated an angle φ, the corresponding matrix becomes a diagonal block matrix in the directions given by φ and ($\varphi + \pi/2$). Thus, the system performs an FRFT of the input object rotated an angle $-\varphi$. In any case, we get the anamorphic FRFT of the input with fractional orders which are functions of the focal lengths of the virtual doublet. Moreover, a change in the angle α results in a new virtual doublet and new fractional orders.

Let us call $(x_{\varphi i}, y_{\varphi i})$, i = 1, 2, the new coordinates after the rotation of angle φ,

$$\begin{pmatrix} x_{\varphi i} \\ y_{\varphi i} \end{pmatrix} = \begin{pmatrix} \cos\varphi & \sin\varphi \\ -\sin\varphi & \cos\varphi \end{pmatrix} \begin{pmatrix} x_i \\ y_i \end{pmatrix} \tag{12}$$

and let us represent by $g_1'(x_{\varphi 1}, y_{\varphi 1})$ the input object referred to the rotated axes and by $g_{2An}'(x_{\varphi 2}, y_{\varphi 2})$ the amplitude distribution at the anamorphic FRFT plane. Let us represent by p_φ and $p_{\varphi+\frac{\pi}{2}}$ the respective fractional orders.

The new ray matrix is

$$\begin{bmatrix} 1-\dfrac{d}{f_A'} & d\left(2-\dfrac{d}{f_A'}\right) & 0 & 0 \\ -\dfrac{1}{f_A'} & 1-\dfrac{d}{f_A'} & 0 & 0 \\ 0 & 0 & 1-\dfrac{d}{f_B'} & d\left(2-\dfrac{d}{f_B'}\right) \\ 0 & 0 & -\dfrac{1}{f_B'} & 1-\dfrac{d}{f_B'} \end{bmatrix} \tag{13}$$

And after generalized Collins formula [25, 41]

$$\begin{aligned} g_{2An}'(x_{\varphi 2}, y_{\varphi 2}) \propto & \exp\left[j\pi \frac{1-\dfrac{d}{f_A'}}{\lambda d\left(2-\dfrac{d}{f_A'}\right)} x_{\varphi 2}^2 \right] \exp\left[j\pi \frac{1-\dfrac{d}{f_B'}}{\lambda d\left(2-\dfrac{d}{f_B'}\right)} y_{\varphi 2}^2 \right] \\ & \iint g_1'(x_{\varphi 1}, y_{\varphi 1}) \exp\left[j\pi \frac{1-\dfrac{d}{f_A'}}{\lambda d\left(2-\dfrac{d}{f_A'}\right)} x_{\varphi 1}^2 \right] \exp\left[j\pi \frac{1-\dfrac{d}{f_B'}}{\lambda d\left(2-\dfrac{d}{f_B'}\right)} y_{\varphi 1}^2 \right] \\ & \exp\left\{ -j2\pi \left[\frac{x_{\varphi 2}}{\lambda d\left(2-\dfrac{d}{f_A'}\right)} x_{\varphi 1} + \frac{y_{\varphi 2}}{\lambda d\left(2-\dfrac{d}{f_B'}\right)} y_{\varphi 1} \right] \right\} dx_{\varphi 1} dy_{\varphi 1} \end{aligned} \tag{14}$$

As could be expected, this equation coincides with the result obtained by direct calculation through Fresnel propagation.

$$\begin{aligned} g_{2An}'(x_{\varphi 2}, y_{\varphi 2}) = & FRFT_{\varphi}^{p_\varphi} FRFT_{\varphi+\frac{\pi}{2}}^{p_{\varphi+\frac{\pi}{2}}} \left[g_1'(x_{\varphi 1}, y_{\varphi 1}) \right] \propto \exp\left(j\pi \frac{x_{\varphi 2}^2}{T_\varphi} \right) \exp\left(j\pi \frac{y_{\varphi 2}^2}{T_{\varphi+\frac{\pi}{2}}} \right) \cdot \\ & \iint g_1'(x_{\varphi 1}, y_{\varphi 1}) \exp\left(j\pi \frac{x_{\varphi 1}^2}{T_\varphi} \right) \exp\left(j\pi \frac{y_{\varphi 1}^2}{T_{\varphi+\frac{\pi}{2}}} \right) \exp\left[-j2\pi \left(\frac{x_{\varphi 1} x_{\varphi 2}}{S_\varphi} + \frac{y_{\varphi 1} y_{\varphi 2}}{S_{\varphi+\frac{\pi}{2}}} \right) \right] dx_{\varphi 1} dy_{\varphi 1} \end{aligned} \tag{15}$$

$$S_\varphi = \lambda f_{1A} \sin\left[p_\varphi \left(\frac{\pi}{2} \right) \right] \tag{16a}$$

$$T_{\varphi} = \lambda f_{1A} \tan\left[p_{\varphi}\left(\frac{\pi}{2}\right)\right] \tag{16b}$$

$$\Phi_{\varphi} = p_{\varphi}\left(\frac{\pi}{2}\right) \tag{16c}$$

$$S_{\varphi+\frac{\pi}{2}} = \lambda f_{1B} \sin\left[p_{\varphi+\frac{\pi}{2}}\left(\frac{\pi}{2}\right)\right] \tag{17a}$$

$$T_{\varphi+\frac{\pi}{2}} = \lambda f_{1B} \tan\left[p_{\varphi+\frac{\pi}{2}}\left(\frac{\pi}{2}\right)\right] \tag{17b}$$

$$\Phi_{\varphi+\frac{\pi}{2}} = p_{\varphi+\frac{\pi}{2}}\left(\frac{\pi}{2}\right) \tag{17c}$$

If we compare Eqs (14) and (15), we obtain

$$T_{\varphi} = \frac{\lambda d\left(2f'_A - d\right)}{f'_A - d} = \lambda f_{1A} \tan\left(\Phi_{\varphi}\right) \tag{18a}$$

$$S_{\varphi} = \frac{\lambda d\left(2f'_A - d\right)}{f'_A} = \lambda f_{1A} \sin\left(\Phi_{\varphi}\right) \tag{18b}$$

$$T_{\varphi+\frac{\pi}{2}} = \frac{\lambda d\left(2f'_B - d\right)}{f'_B - d} = \lambda f_{1B} \tan\left(\Phi_{\varphi+\frac{\pi}{2}}\right) \tag{19a}$$

$$S_{\varphi+\frac{\pi}{2}} = \frac{\lambda d\left(2f'_B - d\right)}{f'_B} = \lambda f_{1B} \sin\left(\Phi_{\varphi+\frac{\pi}{2}}\right) \tag{19b}$$

After some calculations, we have,

$$f_{1A} = \sqrt{d\left(2f'_A - d\right)} \tag{20a}$$

$$f_{1B} = \sqrt{d\left(2f'_B - d\right)} \tag{20b}$$

So,

$$\tan\left(\Phi_{\varphi}\right) = \frac{f_{1A}}{f'_A - d} \tag{21a}$$

$$\tan\left(\Phi_{\varphi+\frac{\pi}{2}}\right) = \frac{f_{1B}}{f'_B - d} \tag{21b}$$

$$\sin\left(\Phi_{\varphi}\right) = f_{1A}/f'_A \tag{22a}$$

$$\sin\left(\Phi_{\varphi+\frac{\pi}{2}}\right) = f_{1B}/f'_B \tag{22b}$$

2.2 Encryption system

The optical setup that we propose consists in two anamorphic fractional Fourier transformers Lohmann's type I in cascade. Each of them is composed of a non-orthogonal cylindrical doublet, the axes

of the cylindrical lenses making a given angle, not necessarily the same in each subsystem. A scheme of the system is shown in Fig 2. The input function to be encoded is $g'_1(x_{\varphi 1}, y_{\varphi 1})$ that can be either real-valued or complex-valued; $g'_{2An}(x_{\varphi 2}, y_{\varphi 2})$ represents the anamorphic fractional Fourier transforms displayed in the output plane of the first subsystem, with fractional orders p_1 and p_2 ; $g'_{\psi 3}(x_{\psi 3}, y_{\psi 3})$ represents the output anamorphic fractional Fourier transform of the second subsystem, with fractional orders p_2 and p_4. The sub-index ψ indicates the angle that the second virtual doublet makes with the coordinate axes, owing to a possible change of the angle between the cylindrical axes of the doublet with respect to the first one. We also denote by M_1 and M_2 the phase functions that are placed at the input plane and at the output plane of the first subsystem, respectively. They can be written as

$$M_1(x_{\varphi 1}, y_{\varphi 1}) = \exp[j2\pi a(x_{\varphi 1}, y_{\varphi 1})] \tag{23}$$

$$M_2(x_{\varphi 2}, y_{\varphi 2}) = \exp[j2\pi b(x_{\varphi 2}, y_{\varphi 2})] \tag{24}$$

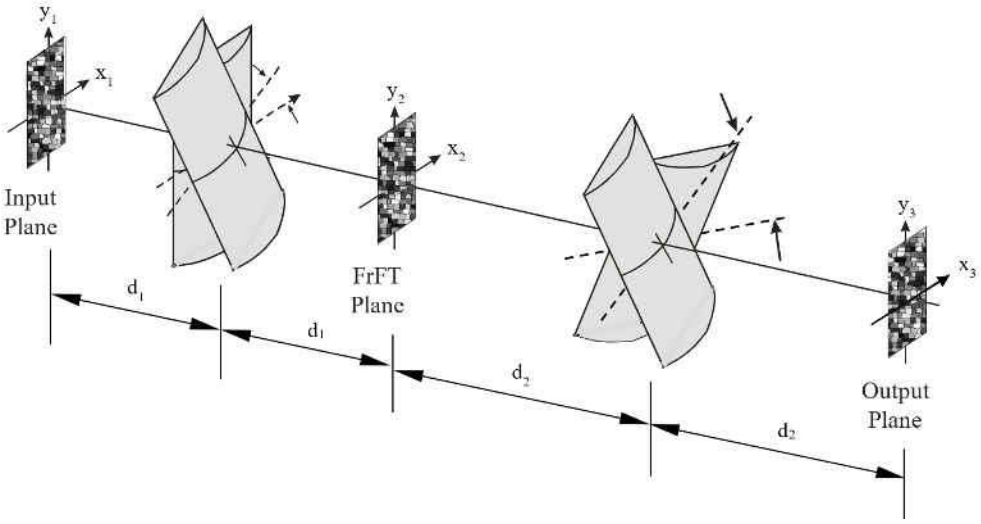

Fig 2. Proposed optical layout for image encryption/decryption based on two anamorphic fractional Fourier transformers Lohmann's type I in cascade.

$a(x_{\varphi 1}, y_{\varphi 1})$ and $b(x_{\varphi 2}, y_{\varphi 2})$ represent two statistically independent white sequences uniformly distributed in the interval [0,1]. In the first subsystem, the input object is multiplied by the mask M_1. We expect that the action of the mask is to provide a white noise image at the first fractional Fourier plane. But owing to the limited bandwidth of the phase mask, we don't obtain that result [38, 14]. Thus, the second mask M_2 is introduced in the fractional Fourier plane. The first virtual orthogonal doublet, equivalent to the first actual subsystem (the cylindrical lenses making an angle α_1), provides the anamorphic FRFT of orders p_1 and p_2 of the complex distribution in the input plane, in the two orthogonal directions given by φ and ($\varphi + \pi/2$); i.e.

$$g'_{2An}(x_{\varphi 2}, y_{\varphi 2}) = FRFT_{\varphi}^{p_1} FRFT_{\varphi+\frac{\pi}{2}}^{p_2}\left[g'_1(x_{\varphi 1}, y_{\varphi 1}) M_1(x_{\varphi 1}, y_{\varphi 1})\right] \tag{25}$$

This complex distribution multiplied by M_2 acts as input image for the second fractional Fourier transformer. If the angle between the cylindrical lenses of the actual doublet is now α_2, the equivalent virtual doublet provides the anamorphic Fourier transforms, of orders p_3 and p_4, in the orthogonal directions given by ψ and ($\psi + \pi/2$) , calculated from Eqs (10a), (10b) and (11). The final encrypted image distribution is

$$g'_{3An}(x_{\psi 3}, y_{\psi 3}) = FRFT_{\psi}^{p_3} FRFT_{\psi+\frac{\pi}{2}}^{p_4}\left[g'_{2An}(x_{\varphi 2}, y_{\varphi 2}) M_2(x_{\varphi 2}, y_{\varphi 2})\right] \tag{26}$$

The encryption keys are the four fractional orders and the two phase masks. The advantage of this system is that with only one change in the angle made by the cylindrical axes of the two lenses in each doublet, we get different fractional orders and, at the same time, we introduce a rotation of the coordinate systems in each of the subsystems. The original angle of the anamorphic cylindrical doublet with regard to the coordinate axes acts as an important additional key too.

For the decryption process we can use the same system as for the encryption but in reverse order and using the conjugates of the masks. The distribution given by Eq (26) is introduced as input image in the second system exchanging the input and output planes and a similar procedure is done in the first system. At the final output plane we obtain the recovered image.

The all-optical experimental implementation of the encryption and the decryption can be carried out by some of the methods proposed in the literature. The phase masks are introduced with spatial light modulators (SLMs). But also, the encrypted image can be obtained digitally and carry out the decryption optically. In that case, the main problem comes from the adjustments of pixelates of the SLMs and that of the digitally encrypted image. However, in this paper we only present computer simulation results to verify the feasibility of the proposed system.

3 Computer simulations

3.1 Orthogonal anamorphic doublets.

To perform the simulation, we assume that our encryption system is like that shown in Fig 3. In order to clarify the behavior of the system, let us begin with orthogonal doublets. The first doublet is composed of two cylindrical lenses, of focal lengths f'_{11} = 300mm and f'_{12} = 500mm ; we represent by α_{11} (named as ANGINI1 in simulations) and $\alpha_{12} = \alpha_{11} + 90^{o}$ the initial angles that the cylinder axes of such lenses make with regard to the x-coordinate axis. The propagation distance is represented d_1 = 300mm. The focal lengths of the second doublet are f'_{21}= 200 mm and f'_{22} = 450mm, the angles with the *x*-axis are represented by α_{21} (named as ANGINI2 in simulations) and $\alpha_{11} = \alpha_{21} + 90^{o}$, and the propagation distance d_2 = 250mm. When the doublets are aligned with the coordinate axis ($\alpha_{11} = \alpha_{21} = 0$) , the fractional orders in the first system are p_{1X} = 1 and p_{1Y} = 0.738, and in the second p_{2X} = 1.161 and p_{2Y} = 0.707. These values maintain along the cylinder axes independently of the orientation of the orthogonal doublet.

The two images to be encrypted and later recovered are shown in Fig 3(a), a picture of the real life, and in Fig 3(b), aone-dimensional (1D) resolution target to check, at least from a qualitative point of view, the loose of resolution in the process.

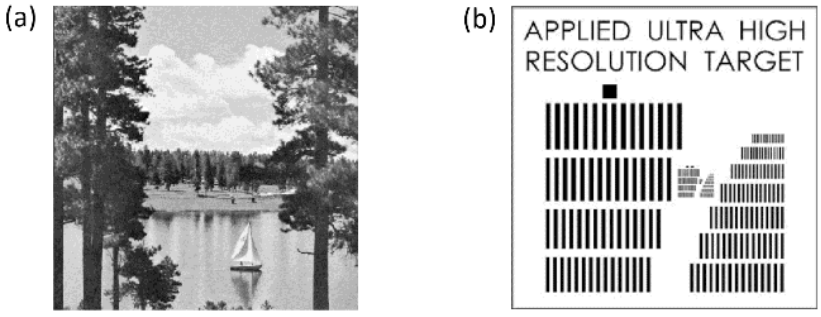

Fig 3. Selected images for simulations: (a) picture of the real life and (b) 1D resolution test target.

We consider that the encryption has been done with angles $\alpha_{11} = \alpha_{21} = 15°$. These angles together with the fractional orders of each system are the keys for the decryption process. The encrypted images

have no features of the original images. To check the performance of the system, we make the decryption in two cases: a) in the first system, we assume that the correct angle $\alpha_{11} = 15°$ is used and, in the second, α_{21} varies in an interval of ±10° around the correct value; and b) in the second system we assume that the correct angle $\alpha_{21} = 15°$ is used and, in the first, α_{11} varies in an interval of ±10°. The deviation angle, β, constitutes in both cases the error of the system in the decryption. When the correct keys are used in the decryption process, we recover the original images, as shown in the center of rows 1 and 3 in Fig 4, corresponding to the value $\beta = 0°$. The decryption sensitivity with respect to the changes introduced by the angle error β can be measured, as usual, by means of the mean squared error (MSE) between the decrypted and the original images. The MSE is given by:

$$MSE = \frac{1}{M \times N} \sum_{i=1}^{M} \sum_{j=1}^{N} \left| I_o(i,j) - I_d(i,j) \right|^2 \tag{26}$$

$I_0\,(i, j)$ denotes the original image and $I_d\,(i, j)$ the decrypted one. M and N are the number of pixels along the x and y axes, respectively.

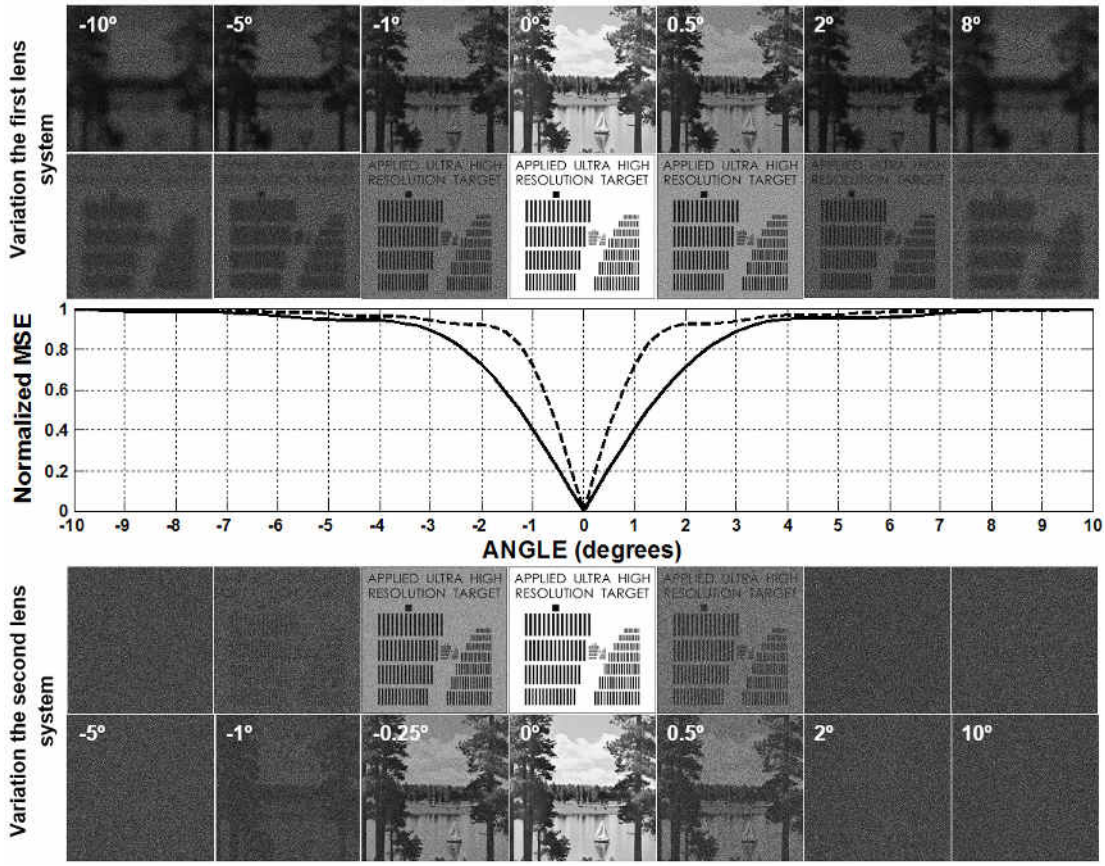

Fig 4. Calculated normalized MSE against the values of the angle β (second row) and decrypted images for determined values of β when an error has been made either in the decryption angle in the first system (continuous line and upper row, respectively) or in the decryption angle in the second system (dashed line and lower row, respectively). For $\beta = 0$, the decryption angles are $\alpha_{11} = \alpha_{21} = 15°$.

Figure 4, row 2, shows the normalized calculated MSE against the values of the angle β, when the error is made in system 2 (dashed line) and in system 1 (continuous line). These plots, as well as the rest of

plots in this section, have been obtained in steps of 0.25°. Row 1 shows the aspect of the decrypted images with the error made in system 1, and row 3 when the error is made in system 2, for determined values of β in order to compare the degradation of the images.

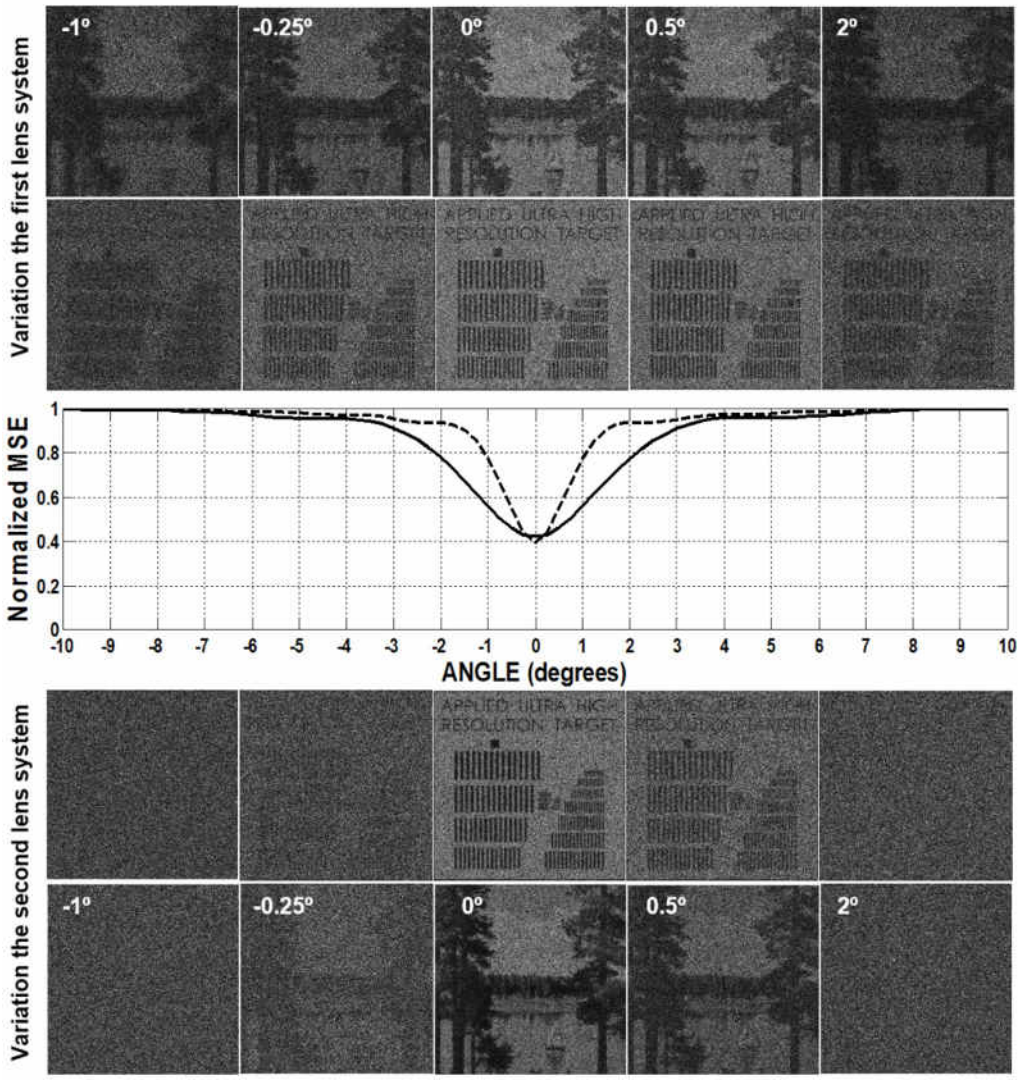

Fig 5. Calculated normalized MSE against the values of the angle β (second row) and decrypted images for determined values of β when an error has been made either in the decryption angle in the first system (continuous line and upper row, respectively) or in the decryption angle in the second system (dashed line and lower row, respectively). Moreover, for β = 0, there is also an initial error either of 1° in the first system (initial decryption angle α_{11} = 16°) or of 0.5° (initial decryption angle α_{21} = 15.5°).

Looking at the two plots of MSE, we realize that the encryption system is more sensitive to errors in the orientation of the second anamorphic system than to errors in the first one. For instance, an error of 0.5° in the second system gives rise to a similar degradation of the images than an error of 1° in the first one, in agreement with the values of the normalized MSE. Moreover, for values greater than 2° in the second

system, there is no decryption, whereas the same error, and even greater, in the first system permits at least a partial decryption. It is worthy to note that the plots of MSE are almost the same for the two images.

Taking into account the different sensitivity of the decryption process to errors in systems 1 and 2, row 2 in Fig 5 displays similar plots to those shown in Fig 4, but the continuous line corresponds to the case in which a permanent error of ±1° has been made in the value of α_{11} in the decryption process, whereas the dashed line corresponds to the case in which a permanent error of ±0.5° has been introduced in the value of α_{21}. As before, rows 1 and 3 show the aspect of the decrypted images for determined values of the angle error β. Owing to the permanent error either in α_{11} or in α_{21} in any case a correct decryption is obtained.

In both curves, for $\beta = 0$, the normalized MSE takes approximately the value 0.4 and increasing values when β differs from zero. Increasing values of MSE implies a greater degradation of the final image.

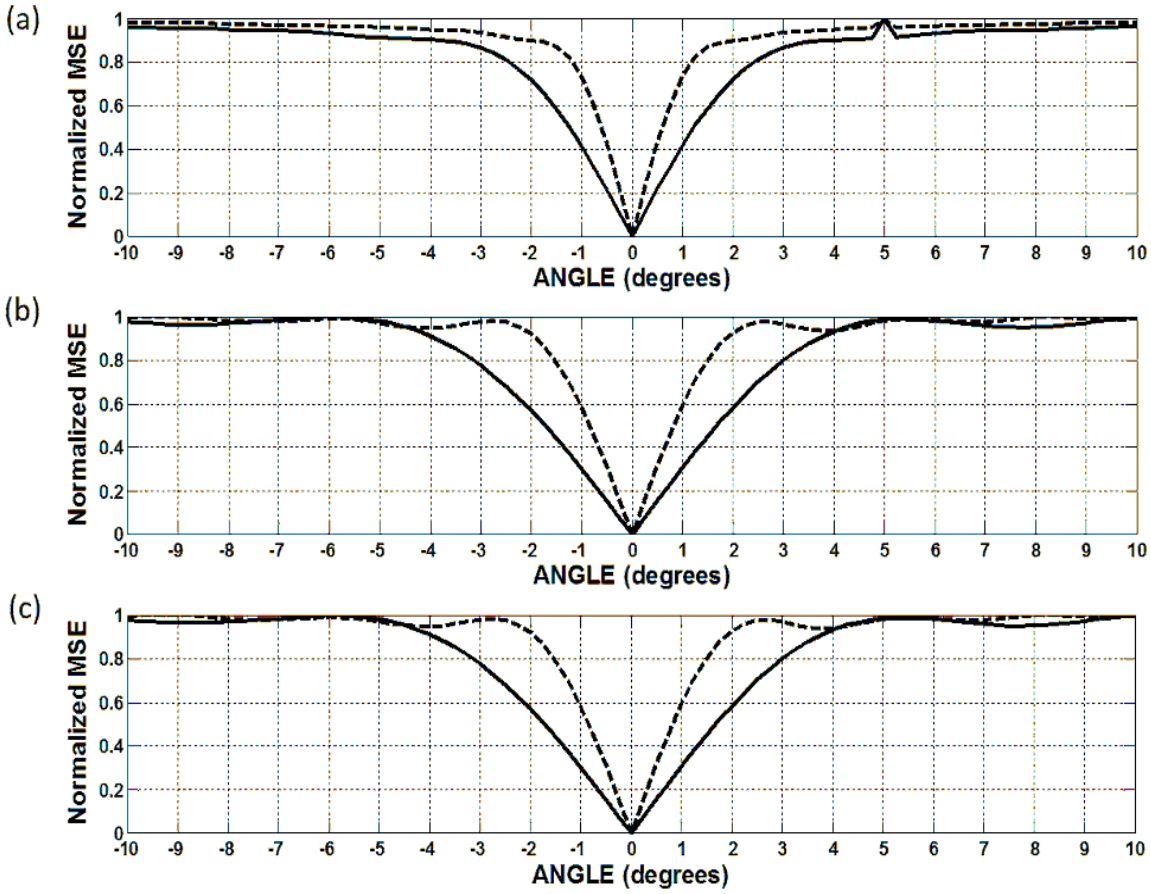

Fig 6. Calculated normalized MSE against the values of the angle β when an error has been made either in the decryption angle in the first system (continuous line) or in the decryption angle in the second system (dashed line). For $\beta = 0$, the decryption angles α_{11} and α_{21} take the correct values in each case. Encryption angles: (a) $\alpha_{11} = \alpha_{21} = 85°$; (b) $\alpha_{11} = \alpha_{21} = 145°$; (c) $\alpha_{11} = \alpha_{21} = 55°$

To study the behavior of the normalized MSE, that is, the degradation of the image, we have considered other values of the angle α_{11} in two cases, (a) when $\alpha_{11} = \alpha_{21}$, and (b) when $\alpha_{11} \neq \alpha_{21}$. Figure 6(a) shows the plot of the normalized MSE against β when $\alpha_{11} = \alpha_{21} = 85°$ and the decryption is made with correct initial angles. Figure 6(b) and Fig 6(c) show analogous plots when $\alpha_{11} = \alpha_{21} = 145°$ and $\alpha_{11} = \alpha_{21} = 55°$, respectively.

As it can be seen, depending on the value of the encryption angles, the curves have different widths, that is, they degrade more in one case than in another, although they are rather similar. For completeness, in Fig 7 we plot the semi-angle deviation around the initial angle necessary to get the 40% of the normalized MSE as a function of its values between 0° and 0180°. As in the previous figures, the continuous line corresponds to variations of α_{11} when the correct value of α_{21} is introduced and the dashed line to variations of α_{21} when the correct value of α_{11} is used. The degradation is quicker when the value of $\alpha_{11} = \alpha_{21}$ is around 90° and slower around 45°.

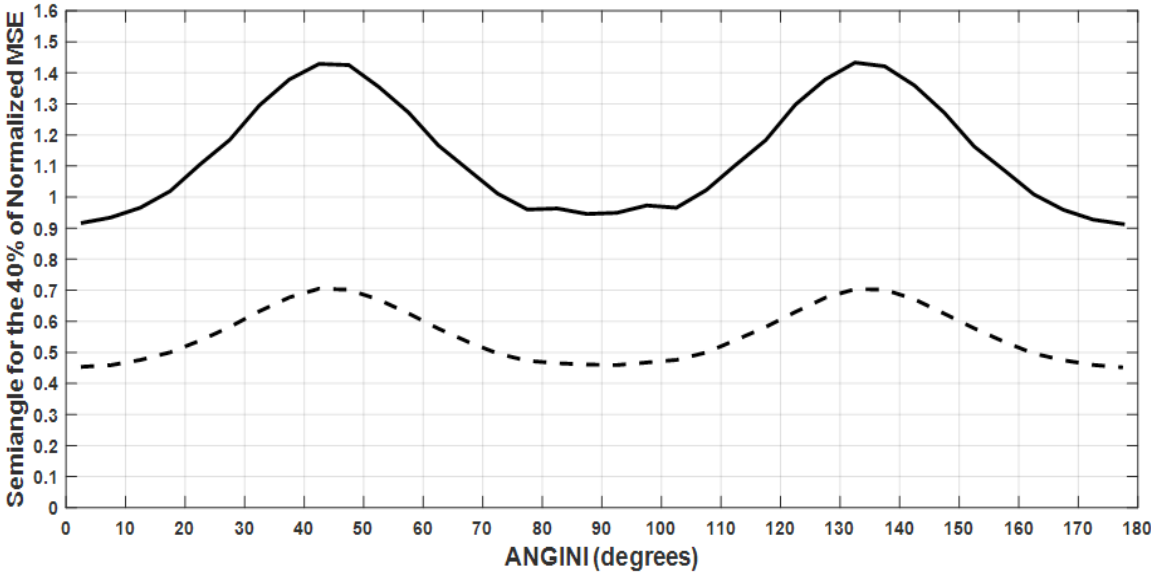

Fig 7. Plot of the semi-angle deviation around the initial angle to obtain 40% of the normalized MSE as a function of the initial angle. The continuous line corresponds to errors in the decryption angle in the subsystem and the dashed line to errors in the second subsystem.

In case that $\alpha_{11} \neq \alpha_{21}$, we obtain similar plots of the normalized MSE against the deviation angle β, but with greater differences in the behavior between the two curves for the different cases selected. Figure 8 shows the plots when: (a) $\alpha_{11} = 15°$, $\alpha_{21} = 55°$, (b) $\alpha_{11} = 15°$, $\alpha_{21} = 85°$; (c) $\alpha_{11} = 15°$, $\alpha_{21} = 140°$; (d) $\alpha_{11} = 45°$, $\alpha_{21} = 140°$; and (e) $\alpha_{11} = 45°$, $\alpha_{21} = 80°$. The behavior of the two subsystems is quite different, the degradation being greater for determined pairs of α_{11} and α_{21} values.

In Fig 9(a) and Fig 9(b) we plot the semi-angle deviation around the initial angle necessary to get the 40% of the normalized MSE as a function of its values between 0° and 180° for the two pairs of values of encryption angles (α_{11}, $\alpha_{21} = \alpha_{11} + 15°$) and ($\alpha_{11}$, $\alpha_{21} = \alpha_{11} + 45°$). As in the previous figures, the continuous line corresponds to variations of α_{11} when the correct value of α_{21} is introduced and the dashed line to variations of α_{21} when the correct value of α_{11} is used.

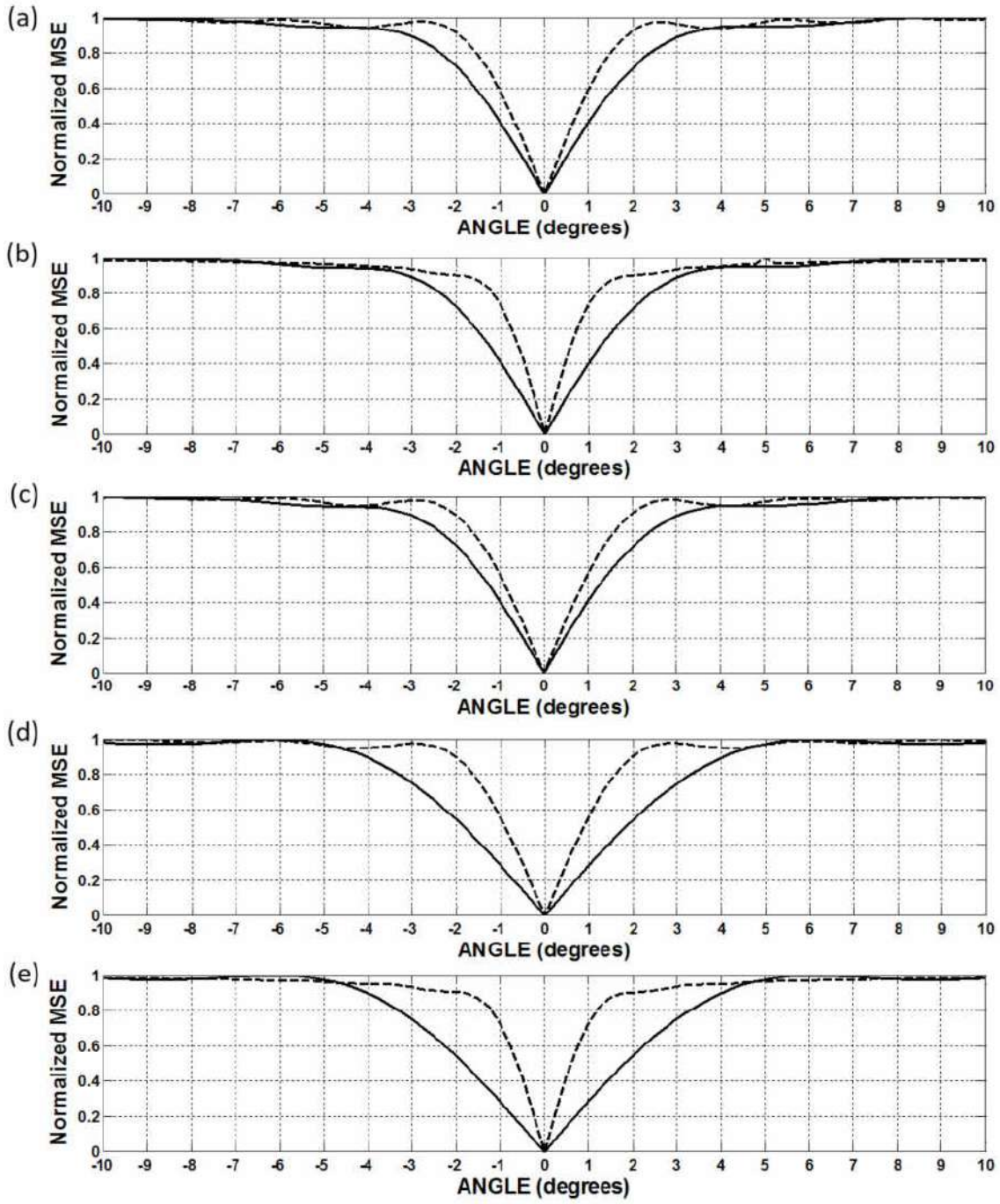

Fig 8. Calculated normalized MSE against the values of the angle β when an error has been made either in the decryption angle in the first system (continuous line) or in the decryption angle in the second system (dashed line). For β = 0, the decryption angles α_{11} and α_{21} take the correct values in each case. Encryption angles: (a) α_{11}= 15°, α_{21}= 55° ; (b) α_{11} = 15°, α_{21} = 85°; (c) α_{11}= 15°, α_{21} = 140°; (d) α_{11} = 45°, α_{21} = 140°; (e) α_{11}= 45°, α_{21} = 80° .

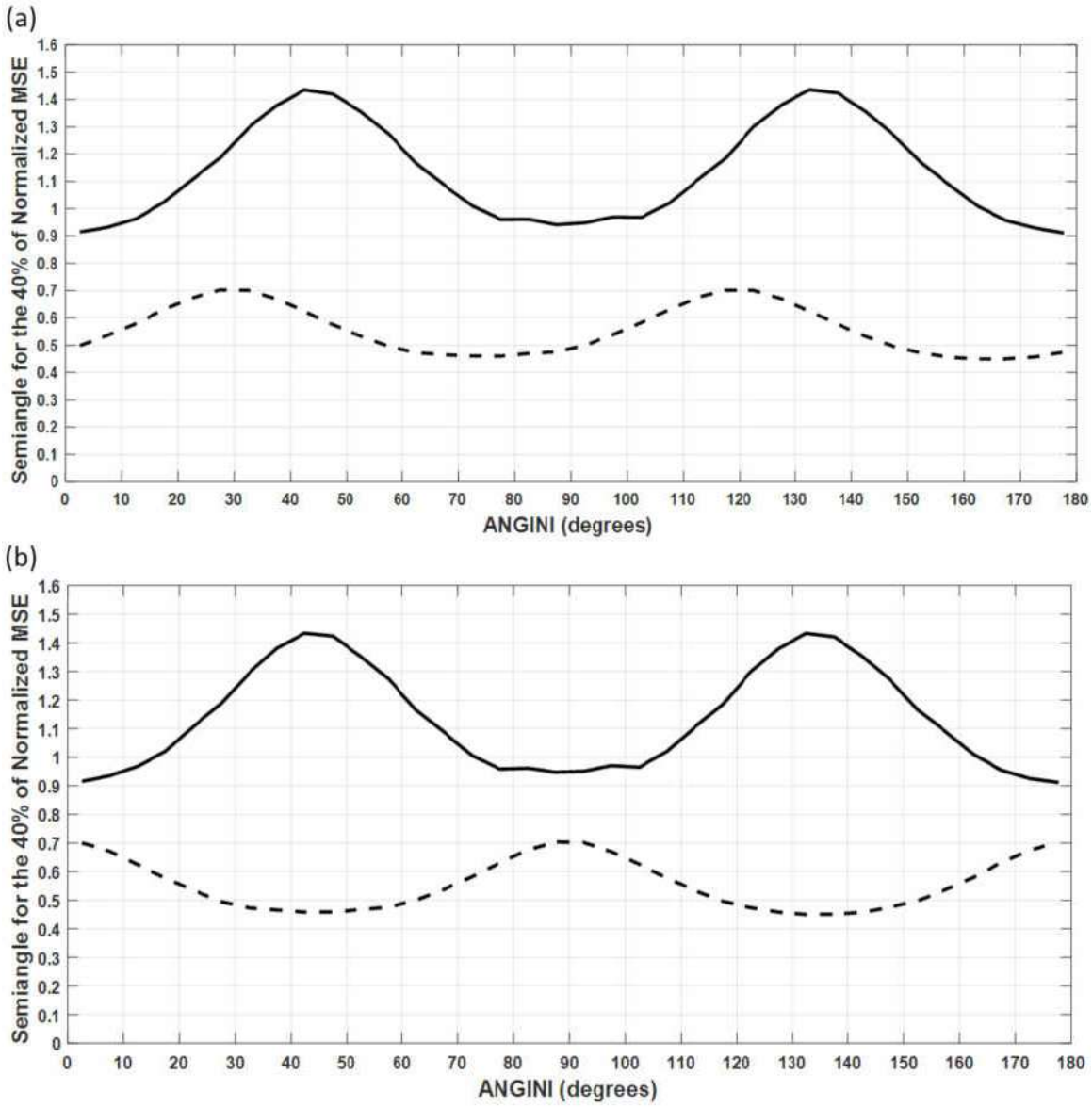

Fig 9. Plot of the semi-angle deviation around the initial angle to obtain 40% of the normalized MSE as a function of the initial angle. The continuous line corresponds to errors in the decryption angle in the first subsystem and the dashed line to errors in the second subsystem. In (a) $\alpha_{21} = \alpha_{11} + 15^{\circ}$; in (b) $\alpha_{21} = \alpha_{11} + 45^{\circ}$

Looking at Fig 9, it can be seen that there is a maximum difference between the curves for the pair ($\alpha_{11} = 45^{\circ}$, $\alpha_{21} = 90^{\circ}$). This means that meanwhile the subsystem two degrades very quickly, the subsystem one does it slowly, as shown in Fig 10(a). On the contrary, the minimum difference between the two curves appears for the pair ($\alpha_{11} = 85^{\circ}$, $\alpha_{21} = 130^{\circ}$) as shown in Fig 10(b). Now, the two subsystems degrade in a close way.

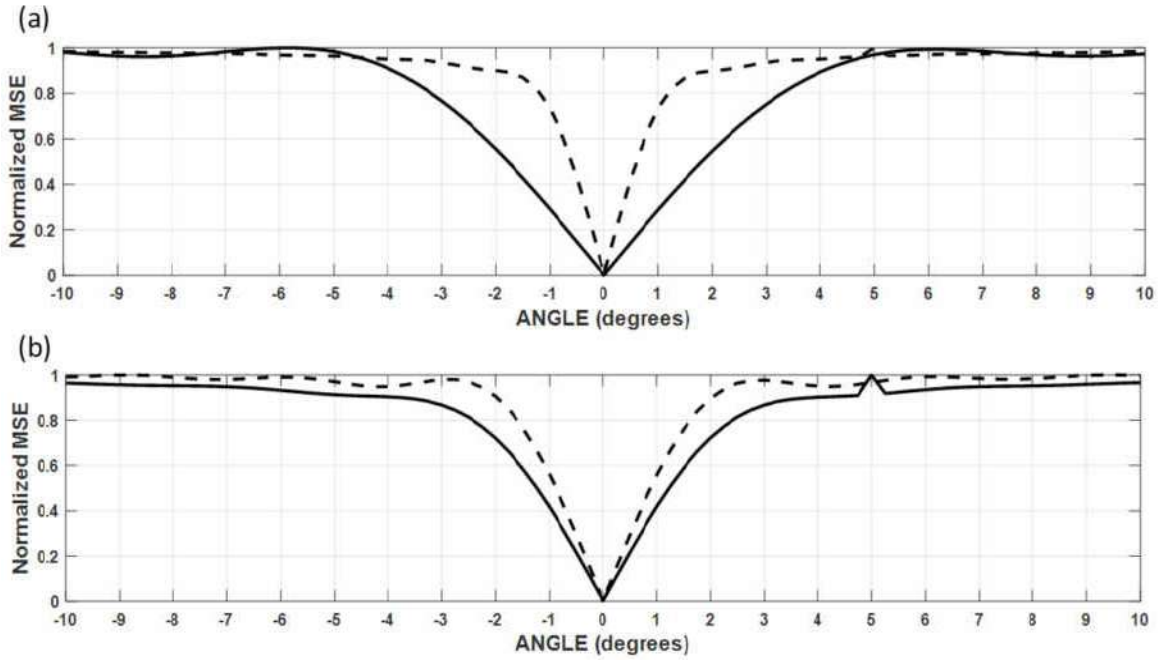

Fig 10. Calculated normalized MSE against the values of the angle β when an error has been made either in the decryption angle in the first system (continuous line) or in the decryption angle in the second system (dashed line). For β = 0, the decryption angles α_{11} and α_{21} take the correct values in each case. Encryption angles: (a) $\alpha_{11} = 45^{\circ}$, $\alpha_{21} = 90^{\circ}$; (b) $\alpha_{11} = 85^{\circ}$, $\alpha_{21} = 130^{\circ}$.

To check the behavior we consider the following cases:

3.2.1 The image is encrypted with $\alpha_{11} = \alpha_{21} = 15^{\circ}$ and, $\delta_1 = \delta_2 = -10^{\circ}$. According to Table 1, the first virtual doublet has the following parameters:

$f_{A1}' = 288\text{mm}$, $f_{B1}' = 537\text{mm}$, $\phi_1 = 27.36^{\circ}$

Table 1.Values of the parameters of the equivalent orthogonal system 1 and the corresponding fractional orders for selected values of α_{11} and δ_1.

$\alpha_{11}(^{\circ})$	$\delta_1(^{\circ})$	$f_{A1}'(mm)$	$f_{B1}'(mm)$	$\varphi_1(^{\circ})$	$d_1(mm)$	$p_{\varphi 1}$	$p_{\varphi 1+\pi/2}$
0	0	300	500	0	300	1.0	0.738
0	–10	288	537	8.94	300	1.026	0.709
15	–10	288	537	27.36	300	1.026	0.709
30	–10	288	537	42.46	300	1.026	0.709
0	–30	243	824	18.29	300	1.151	0.561
15	–30	243	824	33.30	300	1.151	0.561
30	–30	243	824	48.29	300	1.151	0.561
0	–60	200	3000	10.89	300	1.333	0.287
15	–60	200	3000	25.87	300	1.333	0.287
30	–60	200	3000	40,89	300	1.333	0.287

The values of the fractional orders are $p_{\varphi 1} = 1.026$ and $p_{\varphi 1+\frac{\pi}{2}} = 0.709$.

From Table 2, the parameters of the second doublet are:

$f'_{A2} = 198\ mm$

$f'_{B2} = 460\ mm$

$\varphi_2 = 19.10^{o}$

The values of the fractional orders are $p_{\varphi 2} = 1.169$ and $p_{\varphi 2+\frac{\pi}{2}} = 0.698$

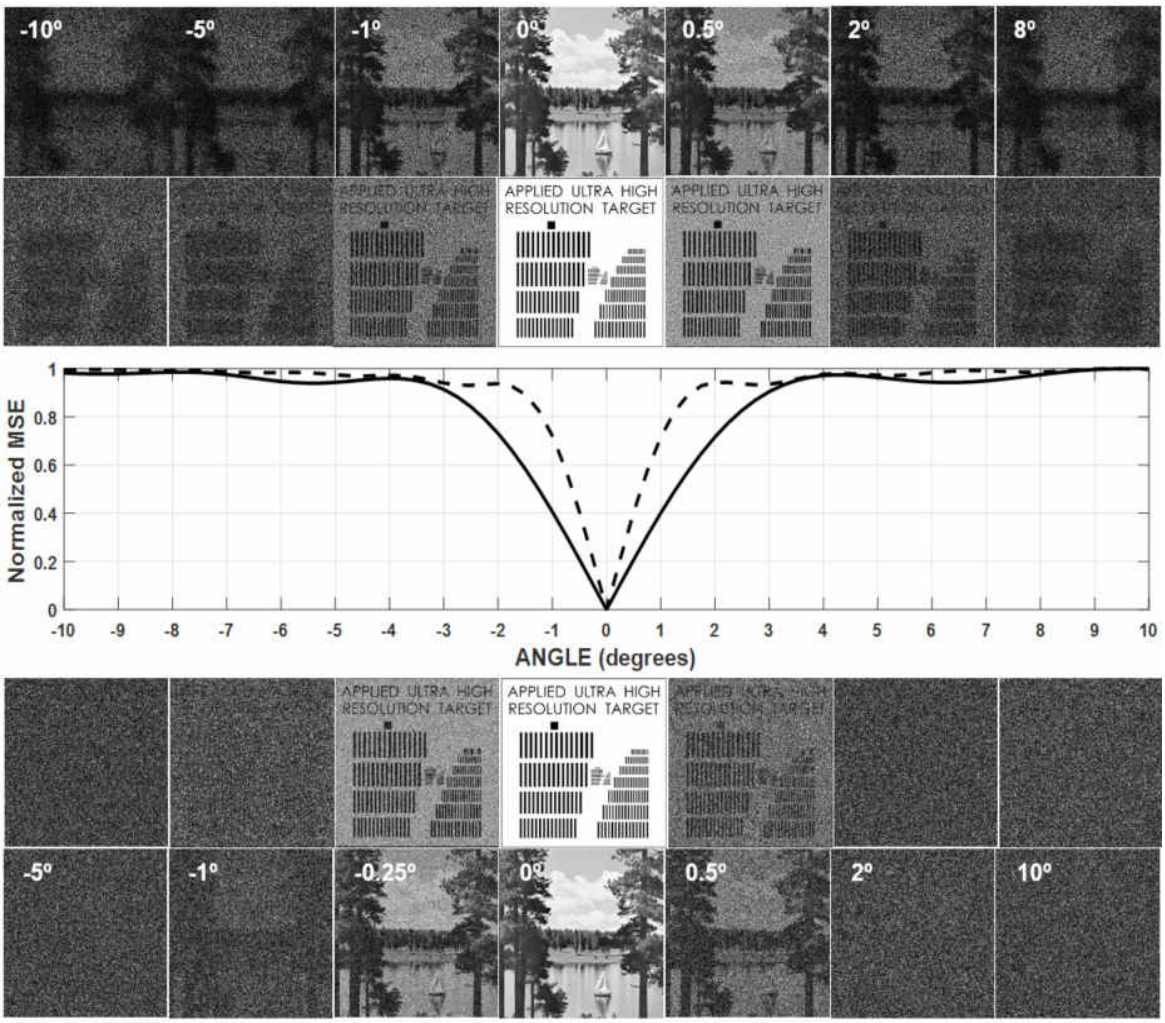

Fig 11. Non-orthogonal doublets. Calculated normalized MSE against the values of the angle β (second row) and decrypted images for determined values of β when an error has been made either in the decryption angle in the first system (continuous line and upper row, respectively) or in the decryption angle in the second system (dashed line and lower row, respectively). For β = 0, the decryption angles are $\alpha_{11} = \alpha_{21} = 15^{o}$. The deviations from orthogonality are $\delta_1 = \delta_2 = -10^{o}$.

Table 2. Values of the parameters of the equivalent orthogonal system 2 and the corresponding fractional orders for selected values of α_{21} and δ_2.

α_{21}	δ_2 (°)	$f'_{A2}(mm)$	$f'_{B2}(mm)$	φ_2 (°)	$d_2(mm)$	$p_{\varphi 2}$	$p_{\varphi 2+\pi/2}$
0	0	200	450	0	250	1.161	0.707
0	–10	198	460	7.31	250	1.167	0.698
15	–10	198	460	19.10	250	1.167	0.698
30	–10	198	460	35.59	250	1.167	0.698
0	–30	185	498	13.17	250	1.229	0.668
15	–30	185	498	18.22	250	1.229	0.668
30	–30	185	498	42.08	250	1.229	0.668
0	–60	147	2457	8.74	250	1.494	0.290
15	–60	147	2457	23.74	250	1.494	0.290
30	–60	147	2457	38.74	250	1.494	0.290

We assume that the only change to be done is the variation of the angle between the two cylindrical lenses in both doublets. Figure 11, row 2, shows the normalized calculated MSE against the values of the angle β, when the error is made in system 2 (dashed line) and in system 1 (continuous line). Row 1 shows the aspect of the decrypted images with the error made in system 1, and row 3 when the error is made in system 2, for determined values of β in order to compare the degradation of the images. For β = 0º, that is, when all the correct keys have been used in the decryption process, correct decrypted images are obtained. As in the case of orthogonal doublets, we realize that the system is more sensitive to angular errors in the second system than in the first one.

3.2.2 The image is encrypted with $\alpha_{11}= \alpha_{21}= 15º$, and $\delta_1 = \delta_2= -60º$. According to Table 1, the first virtual doublet has the following parameters:

$f_{A1}' = 200mm$

$f_{B1}' = 3000mm$

$\varphi_1 = 25.87º$

The values of the fractional orders are $p_{\varphi 1} = 1.333$ and $p_{\varphi 1+\frac{\pi}{2}} = 0.287$.

From Table 2, the parameters of the second doublet are:

$f_{A2}' = 147mm$

$f_{B1}' = 2457mm$

$\varphi_1 = 23.74º$

The values of the fractional orders are $p_{\varphi 2} = 1.494$ and $p_{\varphi 2+\frac{\pi}{2}} = 0.290$

As in the previous figure, Fig 12 shows the plot of the normalized MSE against β and recovered images for selected values of β.

Looking at the plot of the normalized MSE, we realize that when we start with subsystems with great deviations from the orthogonality, the system sensitivity to angular errors in the subsystems is greater than in case of small deviations from the orthogonality.

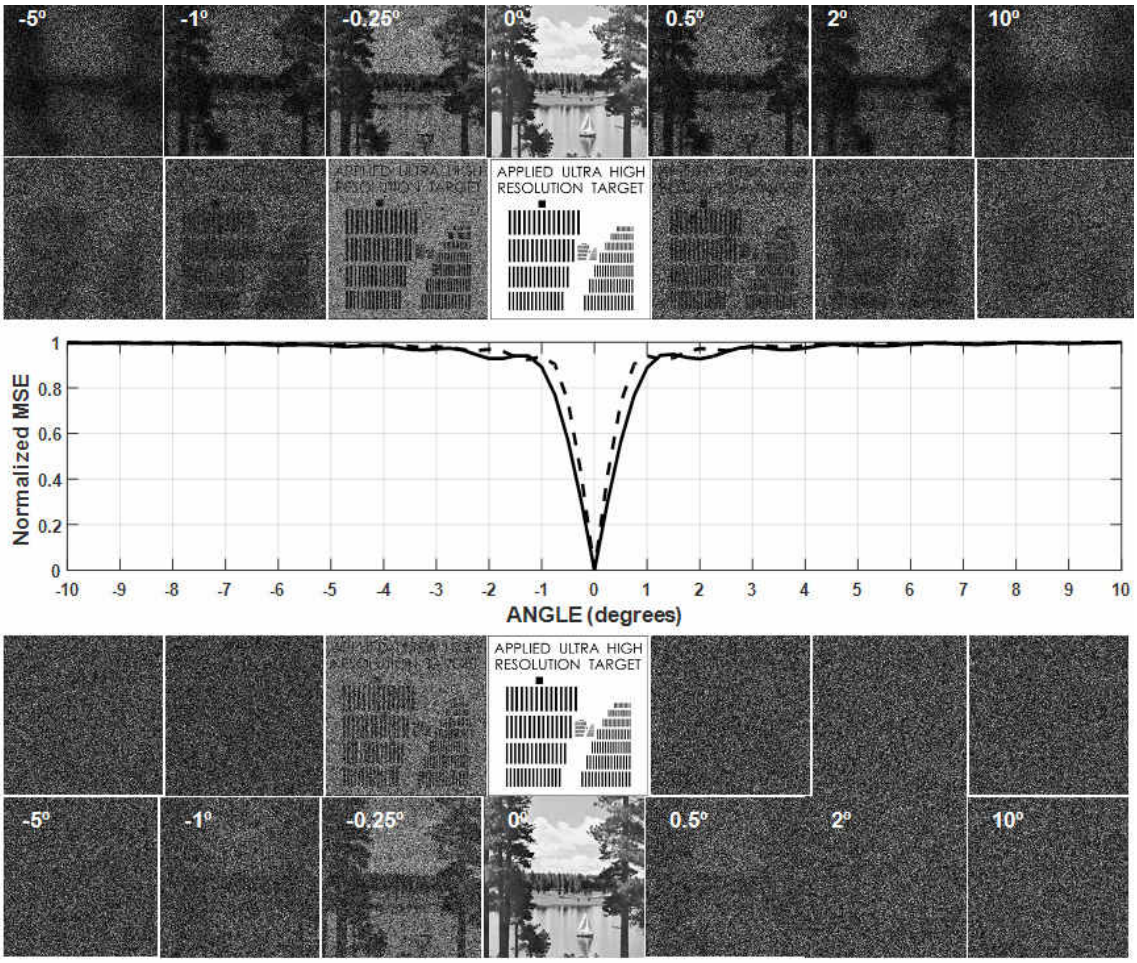

Fig 12. Non-orthogonal doublets. Calculated normalized MSE against the values of the angle β (second row) and decrypted images for determined values of β when an error has been made either in the decryption angle in the first system (continuous line and upper row, respectively) or in the decryption angle in the second system (dashed line and lower row, respectively). For β = 0, the decryption angles are $\alpha_{11} = \alpha_{21} = 15º$. The deviations from orthogonality are $\delta_1 = \delta_2 = -60º$.

3.2.3 We consider now the behavior of the system for given values of the initial angles (ANGINI) when the errors have been made in the deviations from orthogonality, that is, in δ_1 and δ_2. Figure 13 shows the plot of the normalized MSE against δ_1 and δ_2 when they vary ±10° around the values used for encryption. The continuous line corresponds to the case in which δ_1 varies and the correct value of δ_2 is taken, and the dashed line corresponds to variations of δ_2 when the correct value of δ_1 is used. In (a), $\delta_1 = \delta_2 = -10º$; in (b), $\delta_1 = \delta_2 = -30º$; in (c), $\delta_1 = \delta_2 = -60º$; and in (d), $\delta_1 = \delta_2 = -90º$. In all cases, $\alpha_{11} = \alpha_{21} = 15º$.

Looking at Fig 13, we realize that depending on the values of the initial deviations from orthogonality, δ_1 and δ_2, there is a different tolerance in the response of the system to the deviations with regard to the encryption angles in the decryption process. We can see that the tolerance reaches a maximum value and then starts to decrease (for $\delta_1 = \delta_2 = -30º$ the tolerance is lower than for $\delta_1 = \delta_2 = -60º$ and for $\delta_1 = \delta_2 = -90º$ becomes again lower than for $\delta_1 = \delta_2 = -60º$). Moreover, there is almost no difference in the response of the whole system when errors are made either in one or other of the two subsystems. In

order to see the behavior for different deviations angles from orthogonality, we have plotted (see Fig 14) the angular value for which the 40% of the normalized MSE is reached for deviation angles from orthogonality ranging in the interval, $\delta_1 = \delta_2 \in [-90º, 90º]$. Since the response is almost the same in both sub-systems, we have only included a single graph representative of the average from the curves incoming from both sub-systems. Comparing Figs 13 and 14 we can see as the maximum tolerance is reached for –60º and +30º while the minimum is obtained for –15º and 75º, the separation in both cases being 90º.

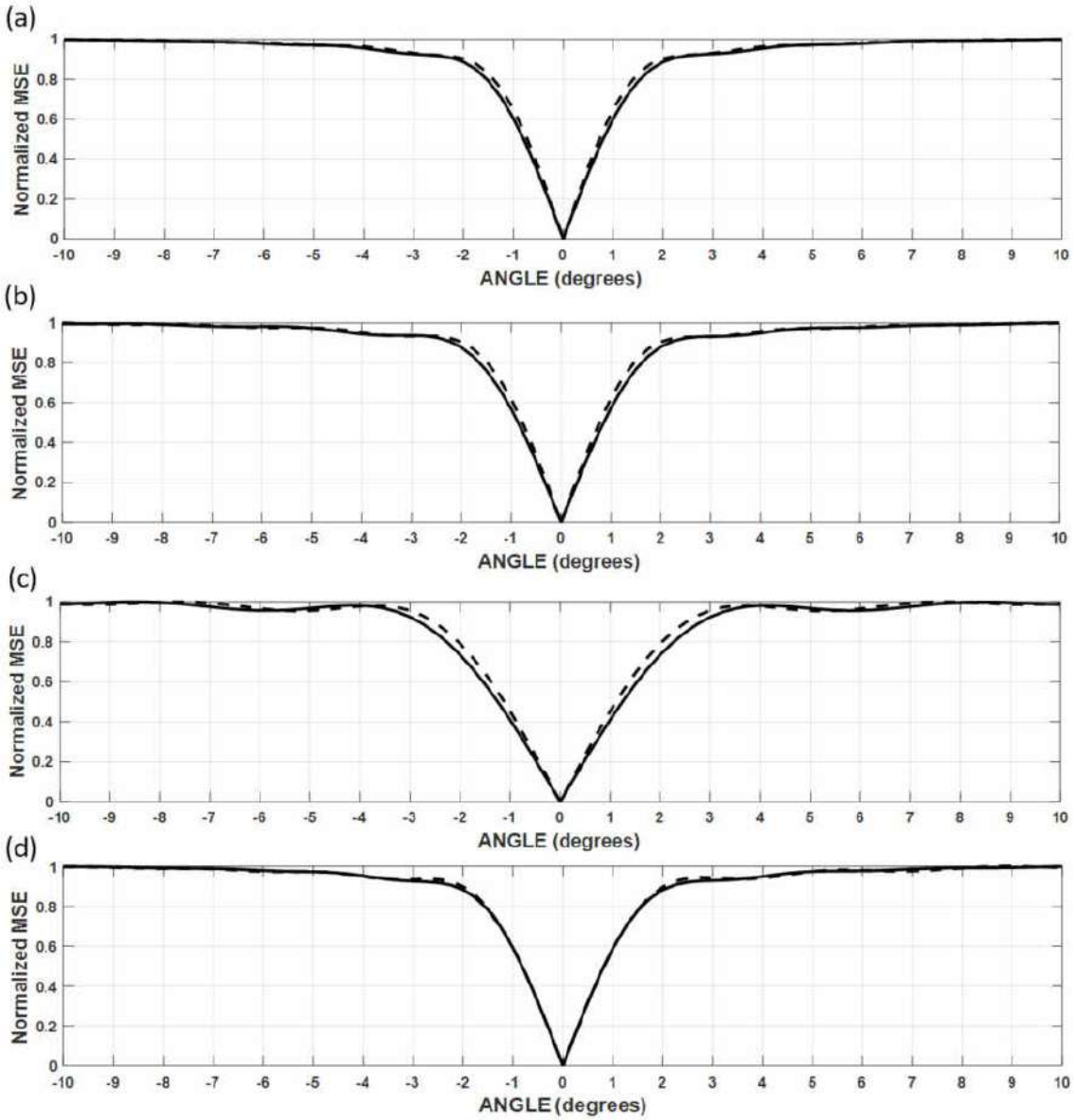

Fig 13. Non-orthogonal doublets. Calculated normalized MSE against the values of δ_1 and δ_2 when they vary ± 10º around the values used for encryption. The continuous line corresponds to the case in which δ_1 varies and the correct value of δ_2 is taken, and the dashed line corresponds to variations of δ_2 when the correct value of δ_1 is used. In (a), $\delta_1 = \delta_2 = -10º$; in (b), $\delta_1 = \delta_2 = -30º$; in (c), $\delta_1 = \delta_2 = -60º$; in (d), $\delta_1 = \delta_2 = -90º$. In the four cases, $\alpha_{11} = \alpha_{21} = 15º$.

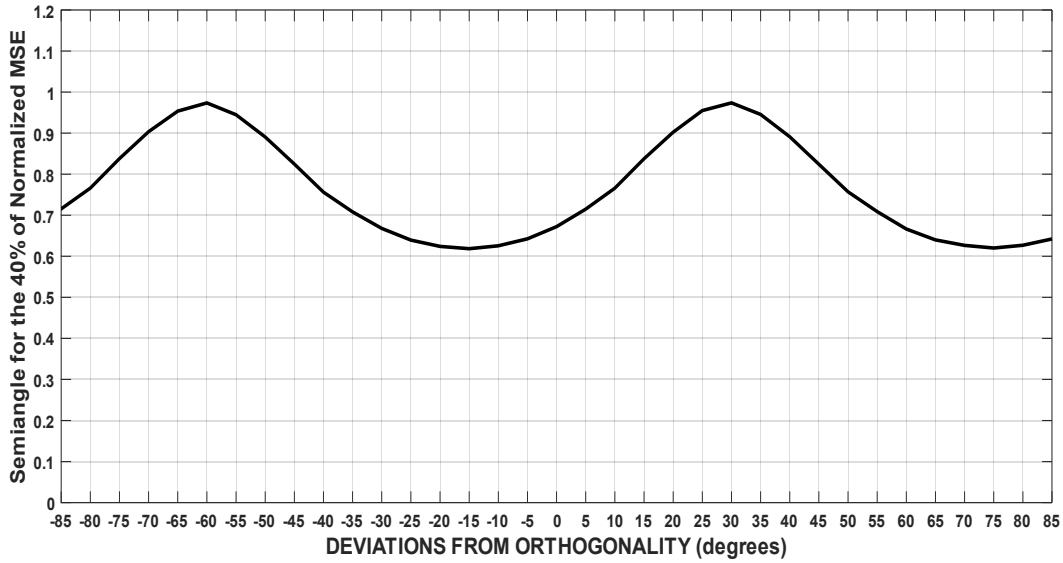

Fig 14. Plot of the angular value for which the 40% of the normalized MSE is reached for deviation angles from orthogonality ranging in the interval $\delta_1 = \delta_2 \in [-90^o, 90^o]$.

Figure 15 considers the case where the initial angles are different (α_{11} = 125º, α_{21} = 55º) and the deviation from orthogonality the same. In (a) $\delta_1 = \delta_2 = -10^o$; in (b) $\delta_1 = \delta_2 = -60^o$. And Fig 16 shows the plot of normalized MSE when both the initial angles and the deviations from orthogonality are different. In this case, still α_{11} = 125º. α_{21} = 55º, but $\delta_1 = -60^o$, $\delta_2 = -10^o$.

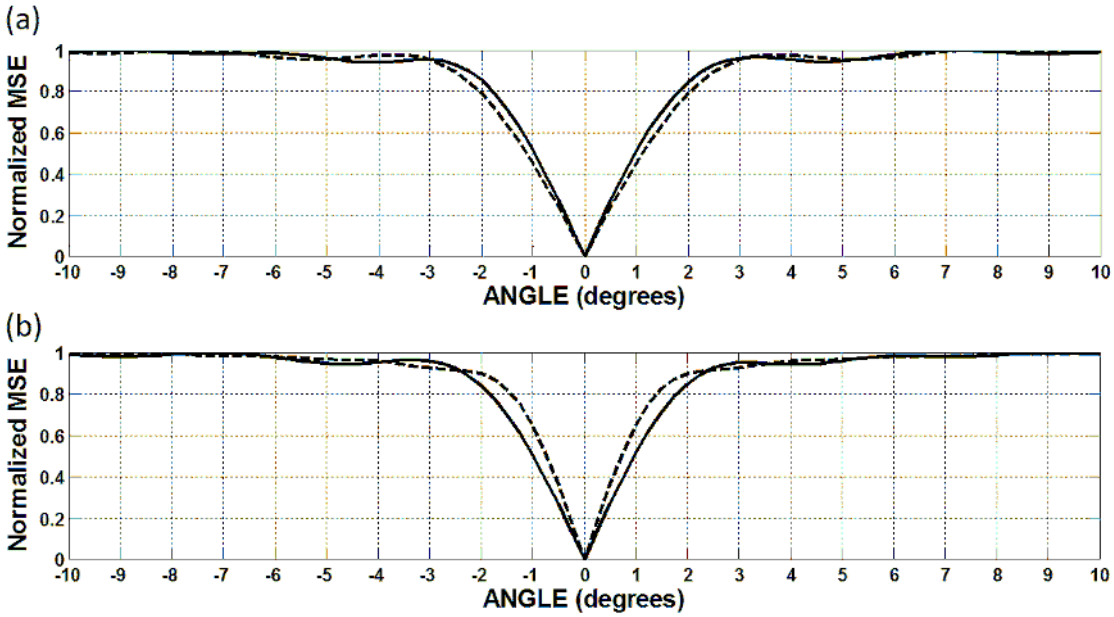

Fig 15. Non-orthogonal doublets. Calculated normalized MSE against the values of δ_1 and δ_2 when they vary ± 10º around the values used for encryption. The continuous line corresponds to the case in which δ_1 varies and the correct value of δ_2 is taken, and the dashed line corresponds to variations of δ_2 when the correct value of δ_1 is used. In (a), $\delta_1 = \delta_2 = -10^o$; in (b) $\delta_1 = \delta_2 = -60^o$. In both cases, α_{11}= 125º, α_{21} = 55º

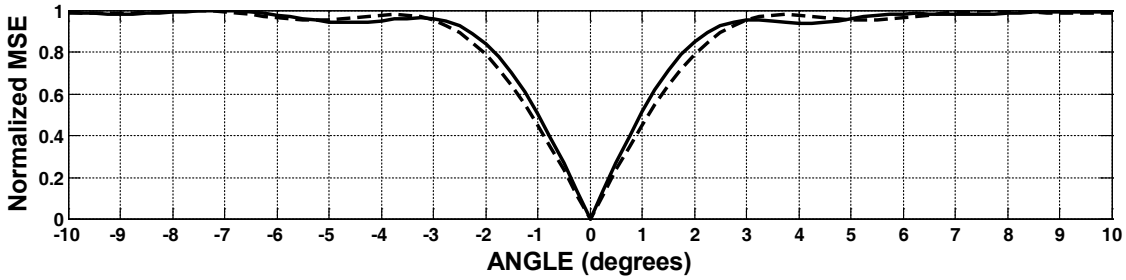

Fig. 16. Non-orthogonal doublets. Calculated normalized MSE against the values of δ_1 and δ_2 when they vary ± 10º around the values used for encryption. The continuous line corresponds to the case in which δ_1 varies and the correct value of δ_2 is taken, and the dashed line corresponds to variations of δ_2 when the correct value of δ_1 is used. $\delta_1 = -60º$, $\delta_2 = -10º$ and $\alpha_{11} = 125º$, $\alpha_{11} = 55º$.

4 Conclusions

Taking into account that a non-orthogonal cylindrical doublet is equivalent to a virtual orthogonal one but rotated with regard to the original coordinate axes, it can be used to build a flexible anamorphic Lohmann's first-type fractional Fourier transformer. The orientation and the focal lengths of the virtual doublet can be changed by simply rotating the angle of one of the cylindrical lenses of the doublet with respect to the other. Notice that this rotation also changes the fractional orders of the virtual doublet. We have analyzed theoretically this behavior.

As an application, we propose the coupling in cascade of two such anamorphic fractional Fourier transformers to perform double random phase encryption. Several layouts of this type can be found in the bibliography but without the flexibility of our proposed system: a simple rotation of one lens is enough to change the fractional orders and, at the same time, to introduce an in-plane rotation of the system.

We present only numerical simulations to substantiate the feasibility of the system. As the non-orthogonal doublet is equivalent to an orthogonal one, we first present results when the encryption and decryption have been performed with systems based on orthogonal doublets. We study the degradation of the decrypted images based on the values of MSE, as usual. We compare the results when angular errors are introduced in each of the sub-systems in the decryption process. In general, the degradation is greater when the errors are made in the second sub-system.

We have also considered the performance as a function of the deviation from orthogonality for systems based on non-orthogonal doublets. In this case, the decryption sensitivity to errors in the first and second systems is quite similar but it depends on the values of the initial angles (ANGINIs) and strongly on the values of the deviation from orthogonality employed to encrypt the images.

Acknowledgements.

Part of this work has been funded by the Spanish Ministerio de Economía y Competitividad and the Fondo Europeo de Desarrollo Regional (FEDER) under the projects FIS2013-47548-P and FIS2012-39158-C02-02.

References

1. Françon M, May M, Correlation and information processing using speckle patterns, *J Opt Soc Am*, 66(1975)1275-1282.
2. Réfrégier Ph, Javidi B, Optical image encryption based on input plane Fourier plane random encoding, *Opt Lett*, 20(1995)767-769.
3. Towghi N, Javidi B, Luo Z, Fully phase encrypted image processor, *J Opt Soc Am A*, 16(1999)1915-1927.

4. Tajahuerce E, Matoba O, Verrall S C, Javidi B, Optoelectronic information encryption with phase-shifting interferometry, *Appl Opt*, 39(2000)2313-2320.
5. Nomura T, Javidi B, Optical encryption system with a binary key code, *Appl Opt*, 39(2000)4783-4787.
6. Matoba O, Javidi B, Encrypted optical storage with wavelength-key and random phase codes, *Appl Opt*, 38(1999) 6785-6790.
7. Matoba O, Javidi B, Encrypted optical storage with angular multiplexing, *Appl Opt*, 38(1999)7289-7293.
8. Tan X, Matoba O, Shimura T, Kuroda K, Javidi B, Secure optical storage that uses fully phase encryption, *Appl Opt*, 39(2000)6689-6694.
9. Tajahuerce E, Javidi B, Encrypting three-dimensional information with digital holography, *Appl Opt*, 39(2000) 6595-6601.
10. Nomura T, Javidi B, Optical encryption using a joint transform correlator architecture, *Opt Eng*, 39(2000)2031-2045.
11. Takeda M, Nakano K, Suzuki H, Yamaguchi M, Encrypted sensing based on digital holography for fingerprint images, *Optics and Photonics Journal*, 5(2015)6-14.
12. Rueda E, Ríos C, Barrera J F, Torroba R, Master key generation to avoid the use of an external reference wave in an experimental JTC encrypting architecture, *Appl Opt*, 51(2012)1822-1827.
13. Unnikrishnan G, Joseph J, Singh K, Optical encryption by double random phase encoding in the fractional Fourier domain, *Opt Lett*, 25(2000)887-889.
14. Unnikrishnan G, Singh K, Double random fractional Fourier-domain encoding for optical security, *Opt Eng*. 39(2000)2853-2859.
15. Lohmann A W, Image rotation, Wigner rotation, and the fractional Fourier transform, *J Opt Soc Am A*, 10(1993) 2181-2186.
16. Mendlovic D, Ozaktas H M, Fractional Fourier transforms and their optical implementation: I, *J Opt Soc Am A*, 10(1993)1875-1881.
17. Ozaktas H M, Mendlovic D, Fractional Fourier transforms and their optical implementation: II, *J Opt Soc Am A*, 10(1993)2522-2531.
18. Ozaktas H M, Mendlovic D, Fourier transforms of fractional order and their optical implementation, *Opt Commun*, 101(1993)163-169.
19. Bernardo L M, Soares O D D, Fractional Fourier transforms and imaging, *J Opt Soc Am A*, 11(1994)2622-2626.
20. Lohmann A W, A fake zoom lens for fractional Fourier experiments, *Opt. Commun*, 115(1995)437-443.
21. Bernardo L M, ABCD matrix formalism of fractional Fourier optics, *Opt Eng*, 35(1996)732-740.
22. Lohmann A W, Mendlovic D, Zalevsky Z, Fractional transformations in optics, *Prog Optics*, 38(1998)236-343.
23. Moreno I, Davis J A, Crabtree K, Fractional Fourier transform optical system with programmable diffractive lenses, *Appl Opt*, 42(2003)6544-6548.
24. Moreno I, Sánchez-López M M, Ferreira C, Mateos F, Fractional Fourier transform, symmetrical lens systems and its cardinal planes, *J Opt Soc Am A*, 24(2007)1930-1936.
25. Collins S A, Lens-system diffraction integral written in terms of matrix optics, *J Opt Soc Am*, 60(1970)1168-1177.
26. Zhang Y, Zheng Ch-H, Tanno N, Oprtycal encryption based on iterative fractional Fourier transform, *Opt Commun*, 202(2002)277-285.
27. Liu Z, Liu S, Double image encryption based on iterative fractional Fourier transform, *Opt Commun*, 275 (2007)324-329.
28. Situ G, Zhang J, Double random-phase encoding in the Fresnel domain, *Opt Lett*, 29(2004)1584-1586.
29. Wang Q, Guo Q, Lei L, Zhou J, Optical image encryption based on joint fractional transform correlator architecture and digital holography, *Opt Eng*, 52(2013)048201.1-7.

30. Zhong Z, Chang J, Shan M, Hao B, Fractional Fourier-domain random encoding and pixel scrambling technique for double image encryption, *Opt Commun*, 285(2012)18-23.
31. Wang Q, Guo Q, J Zhou, Double image encryption based on linear blend operation and random phase encoding in fractional Fourier domain, *Opt Commun*, 285(2012)4317-4323.
32. Liu S, Guo Ch, Sheridan J T, A review of optical image encryption techniques, *Opt & Laser Tech*, 57(2014)327-342.
33. Mendlovic D, Bitran Y, Dorsch R, Ferreira C, García J, Ozaktas H M, Anamorphic fractional Fourier transform: optical implementation and applications, *Appl Opt*, 34(1995)7451-7456.
34. Sahin A, Ozaktas H M, Mendlovic D, Optical implementation of the two-dimensional fractional Fourier transform with different orders in two dimensions, *Opt Commun,* 120(1995)134-138.
35. García J, Mendlovic D, Zalevsky Z, Lohmann A W, Space-variant simultaneous detection of several objects by the use of multiple anamorphic fractional Fourier transform filters, *Appl Opt*, 35(1996)3945-3952.
36. Moreno I, Ferreira C, Sánchez-López M M, Ray matrix analysis of anamorphic fractional Fourier systems, *J Opt: Pure Appl Opt*, 8(2006)427-435.
37. Unnikrishnan G, Joseph J, Singh K, Fractional Fourier domain encrypted holographic memory by use of an anamorphic optical system, *Appl Opt*, 40(2001)299-306.
38. Kumar P, Joseph J, Singh K, Double random phase encryption with in-plane rotation of a modified Lohmann's second-type system in the anamorphic fractional Fourier domain, *Opt Eng*, 47(2008)117001.1 –7.
39. Long W T, A matrix formalism for decentration problems, *Am J Optom & Physiol Opt*, 53(1976)27-33.
40. Macukow B, Arsenault H H, Matrix decompositions for nonsysmmetrical optical systems, *J Opt Soc Am*, 73(1983)1360-1366.
41. Moreno I, Ferreira C, Fractional Fourier transforms and geometrical optics, in Advances in Imaging and Electron Physics, Vol 161, (Elsevier Inc., Amsterdam), 2010, pp. 89-146.

[*Received*: 7.11.2015]

Dr. Carlos Ferreira, born in Madrid in 1947, is Full Professor of Optics at the University of Valencia (Spain) since 1990. He received the degree in Physics and the PhD in Physics in 1969 and 1972, respectively, at the University of Valencia. He has performed research stays at the University of Warsaw (Poland), the Université Laval (Québec, Canada) and Bar-Ilan University (Israel).

He has carried out research in the fields of pattern recognition, holography, digital and optical processors, Fourier optics, optical systems and super-resolution. This research has produced more than 150 articles published most of them in both peer reviewed journals and also in extended proceedings. He has been supervisor or co-supervisor of 19 Master Thesis and 11 Ph D Thesis.

At the University of Valencia he has had a long and fruitful trajectory serving the institution in several positions. Among them we may highlight his appointments as Member of the Senate, Head of the Optics Department of the Faculty of Physics, Dean of the Faculty of Physics, and Vice-rector for Teaching Staff.

He received the grades of Fellow Member from SPIE (2008) and from OSA (2015). He is also member of EOS – European Optical Society, of RSEF – the Royal Spanish Physical Society, and of SEDOPTICA – the Spanish Optical Society. At SEDOPTICA we may highlight his appointments as President of the Image Techniques Committee (1998-2001) and President of the Society (April 2008 – April 2011).

Vicente Micó received the MS degree in Physics from the Universitat de Valencia in 1999 and the BS degree in Optics and Optometry in 2000. He obtained his Ph.D. in Physics in 2008 at the Universitat de Valencia. After a 9-years period (from 2000 to 2009) working in AIDO (Technological Institute of Optics, Color and Imaging), he joined the Optics Department at the University of Valencia where where he currently holds a Ph D Assistant Professor position. Briefly, his research interests are in two areas. As physicist, he is actively working in optical metrology, digital holography, digital holographic microscopy and optical superresolution, including vibration and deformation metrology, speckle applications, lensless coherent imaging and setups based on spatial light modulators. As optometrist, he is working in theoretical aspects on physiological and visual optics as well as in the development of novel optometric instruments for the measurement of ocular parameters.

Dr Pascuala Garcia-Martinez received her BS degree in physics in 1993 from the University of Valencia, Spain. She received her MS and PhD degrees from the same university in 1995 and 1998, respectively. Since 2002 she is an associate professor in the Department of Optics of the University of Valencia and since 2012 she has been accredited to full Professor of Optics.

Dr Garcia-Martinez's major research interests include optical image processing, pattern recognition and spatial light modulators, specifically liquid crystals applied to diffraction and polarization. She has published more than 55 papers in peer-reviewed journal of impact factor and co-authored 6 chapters of various books. She has participated in more than 70 international and national meetings (11 of them as invited and 1 as plenary). She has collaborated in more than 20 research projects by public funds. Moreover, she also has been involved in private companies as consultant.

She was recognized as SPIE (International Society for optics and photonics founded in USA in 1955) Senior member in 2010 and Senior memberof OSA (Optical Society of America) in 2015.

She is also an active defender of gender actions in science, and has leaded a regional node of the Asociación de MujeresInvestigadoras y Tecnólogas (AMIT) from 2005 to 2007. She is the secretary of the Women in Physics specialized group of the Real Sociedad Española de Física (RSEF). Currently she is member of the Comission for Equality Policies of the University of Valencia, and she presides the gender equality commission of the Faculty of Physics.

Dr Ignacio Moreno is Professor of Optics at University Miguel Hernández, Elche (Spain). He received the degree in Physics and the Ph D in Physics in 1992 and 1996, respectively, at the Autonomous University of Barcelona. For two years (1996-98) he joined the Department of Optics of the University of Valencia, and since 1998 he is at the Department of Materials Science, Optics & Electronics Technology at University Miguel Hernández – UMH.

He is an expert in the field of liquid cristal based optical modulators, and their applications in diffractive and polarization optics. He has published approximately 120 articles in peer reviewed journals.

He received the grades of Senior Member from SPIE – The International Society for Optics and Photonics (2009), Senior Member from OSA – Optical Society of America (2010), and Fellow Member from SPIE (2014). In 2012 he received the EOS2012 Prize from the EOS – EuropeanOptical Society.

In the period 2005-2014 he was editor of the Journal *Óptica Pura y Aplicada* – OPA. In 2014 he became Vice-President of SEDOPTICA. In 2009- 2011 he was member of the SPIE Publications Committee. And since 2013 he is associate editor of the Journal *Optical Engineering*.

Javier Garcia received his B.Sc. and Ph.D. in Physics by the Universitat de Valencia in 1989 and 1994 respectively. Nowadays he is full Professor in Optics at the Universitat de Valencia, Spain, since 2008. His activity roots in optical image processing and interferometry. He has published over 100 papers on peer reviewed journals and several patents. The research lines have been on speckle interferometry, holography and optical pattern recognition. At present the main activities are centered on remote vibration measurements, 3D image description and optical superresolution imaging.

Zeev Zalevsky received his B.Sc. and direct Ph.D. degrees in electrical engineering from Tel-Aviv University in 1993 and 1996 respectively. Zeev is currently a full Professor in the faculty of engineering in Bar-Ilan University, Israel. His major fields of research are optical super resolution, biomedical optics, nano-photonics and electro-optical devices, RF photonics and beam shaping.

Zeev has published more than 400 refereed journal papers (including papers in journals such as Progress in Optics, Nano Letters, Nano scale, Scientific Reports, Nature Photonics, Nature Communication etc), more than 200 conference proceeding papers, more than 400 international presentations many of which were invited or plenary, 40 issued patents, 6 authored books, 3 books as an editor and 27 book chapters.

For his work Zeev has received various awards such as the ICO (International Commission of Optics) prize, Krill award, the Juludan prize, SAOT (School for Advanced Optical Technologies) young researcher prize, Taubenblatt prize, the young investigator award in nanoscience and nanotechnology given by the Israel National Nanotechnology Initiative together with the ministry of economics, the Image Engineering Innovation Award of the Society for Imaging Science and Technology (IS&T), the Outstanding Young Scientist Award (OYSA) of NANOSMAT, the serial innovator award and more.